Zeitschrift: IABSE reports = Rapports AIPC = IVBH Berichte
Band: 75 (1996)

Rubrik: Session 4: Tests and analysis of connections

SESSION 4

TESTS AND ANALYSIS OF CONNECTIONS

Leere Seite
Blank page
Page vide

Practical Design Method for Semi-Rigid Composite Joints with Double Web Cleat Connections

Michel CRISINEL
Civ. Eng., Section Leader
Swiss Federal Institute
of Technology (EPFL)
CH-1015 Lausanne
Switzerland

Ping REN
Ph. D. Civ. Eng.
Commercial Intertech SA
L-9202 Diekirch
Luxemburg

Alberto CARRETERO
Civ. Eng., Research Assistant
Swiss Federal Institute
of Technology (EPFL)
CH-1015 Lausanne
Switzerland

Abstract

This paper presents a practical and simple method for the prediction of bilinear moment-rotation characteristics of composite beam-to-column joints using double web cleat connections. This method is similar to an existing one for composite joints with end plate connections based on models for the plastic analysis of composite cross-sections. It is verified by comparison to experimental results and computer simulation results based on non-linear finite element analysis. These comparisons demonstrate good and conservative predictions of the semi-rigid behaviour of composite joints with standard steel beam-to-column double web cleat connections.

1. Introduction

Current design practice for steel building frames normally considers beam-to-column joints as either pinned or rigid (Fig. 1). Frames are thus either pin-jointed and require diagonal bracing or rigid and do not in general need to be braced.

Pinned beam-to-column joints transfer principally shear forces with perhaps a small axial force. For this reason these joints are designed such that only the web of a beam is connected to a column. One of the most popular types of connection used in these pinned joints is the bolted double web cleat, with the following advantages :

- fabrication tolerances can be absorbed by the play in bolt holes,
- straight cuts at the ends of beams,
- welds are not required,
- simple erection.

Rigid beam-to-column joints transfer a bending moment, shear force and an axial force. A common type of connection is an end plate, welded to the end of the beam, which is bolted to the column. Fabrication and erection is more complicated in comparison to a pinned beam-to-column joint if a completely rigid joint is required. In many cases it can be necessary to add stiffeners and to reinforce the column web. Nevertheless, rigid beam-to-column joints also have certain practical advantages :

- straight cuts at the ends of beams,
- end plates can be attached with fillet welds and no special treatment of cut ends of beams is needed,

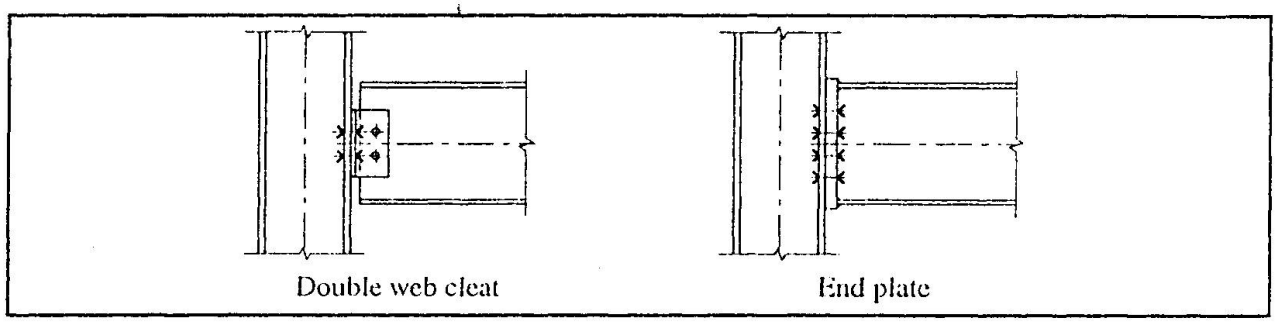

– simple erection.

Fig. 1. Typical steel beam-to-column joints.

Floor slabs in traditional steel building frames are either of reinforced concrete or composite construction and are linked to beams with shear connectors. These slabs are continuous over the region of a beam-to-column joint and have therefore a significant influence on the behaviour of the beam-to-column joint. This influence is greatest in the case of a so-called pinned connection, for which the presence of continuous slab reinforcement has been demonstrated to provide the following advantages :

– increase in the moment resistance of the joint, leading to a reduction in midspan moment,
– higher rigidity of the joint reduces rotation at the column as well as midspan deflection.

In practice the majority of joints are therefore semi-rigid with partial resistance. The semi-rigid behaviour of a joint, somewhere between pinned and completely rigid, influences the distribution of load effects throughout a frame and should be considered during structural analysis.

The contribution of the floor slab is thus very important since it can justify a reduction in material (a lighter beam can be used) whilst employing a simple and economic connection (a double web cleat) as well as traditional construction methods (a composite or reinforced concrete floor slab).

The aim of this contribution is to give a simple and practical hand calculation method to determine the bilinear characteristics used in the design of semi-continuous composite structures.

2. Double web cleat connections

Both types of joint mentionned above have been standardized in Switzerland [1] and in many other countries. This standardization reduces the number of variations, has enabled the development of design tables and simplifies the fabrication of standard elements used in the connections.

Bolted double web cleat connections are both practical and economic. This type of connection can be used between cross and main beams as well as between main beams and columns. In the latter case the connection can be made to either the web or flange of a column (Fig. 2).

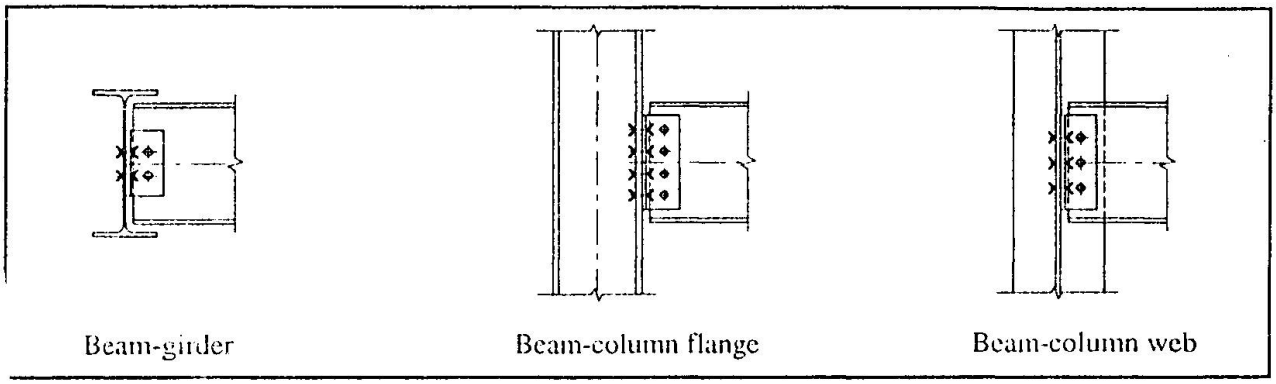

Fig. 2. Three typical double web cleat connections.

Since double web cleat connections have a wide range of application, standard configurations are used in order to simplify design, detailing and fabrication. For each configuration, design tables provide the following data :

- section size and cleat length,
- number, diameter and position of bolt holes,
- thickness of the connecting web or flange,
- vertical shear resistance.

Figure 3 shows several examples of composite beam-to-column joints of different sizes using the standard web cleats mentioned above.

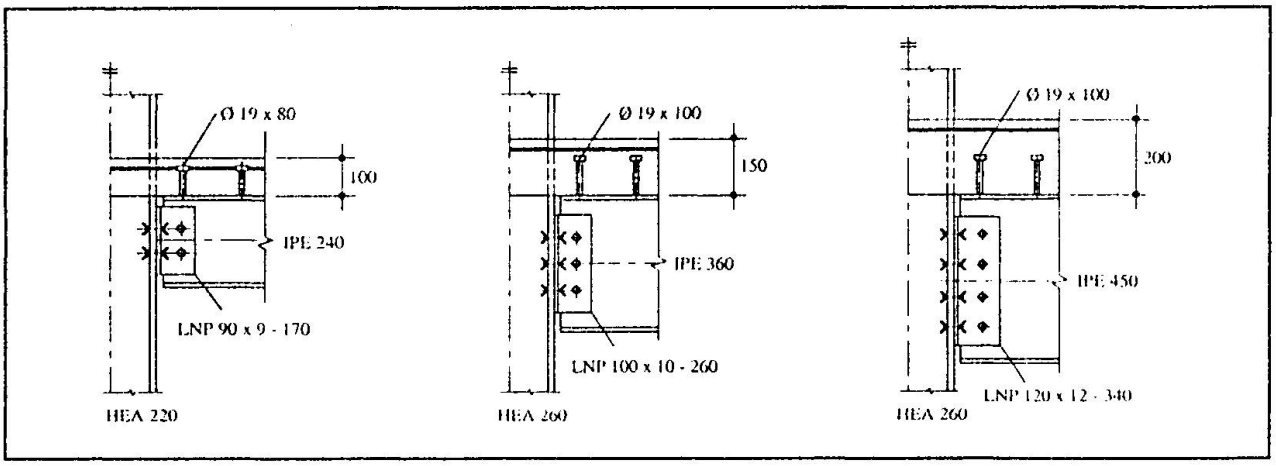

Fig. 3. Typical detailing of composite joints with double web cleat connections.

3. Experimental and analytical investigations

The behaviour of the steelwork connection of a composite joint is more complex than that of a bare steel connection. It is subjected to a very high axial force transferred by the shear connectors between the concrete slab and the steel beam. Existing knowledge about the moment-rotation behaviour of steel connections with the effect of axial force was very poor, so further research was undertaken [2]. Both experimental and analytical studies have been conducted as

part of this research, and tests have been performed on bare steel connections as well as composite joints.

The first part of the research treated bare beam-to-column joints without composite slabs but with the effect of axial force. In this way, the contribution of the bare steelwork connection of a composite joint was assessed, using tests and an analytic approach. The second part of the research treated composite joints. The purpose was to verify the assumption that composite action increases both the strength and stiffness of bare steel joints.

A macro element model of composite joints has been developed and implemented in a computer program. Comparisons between test results and calculation predictions have been made to demonstrate the validity of this numerical model.

3.1 Steel connection tests

Four kinds of loading arrangement were used to apply different moment and axial load combinations to the steel connection. The loading arrangement is shown in Figure 4, together with the test specimen, the test set-up and the test results. Test results in terms of moment-rotation curves for the first three loading arrangements ($\alpha = 90°$, 60° and 30° or N = 0, 0.5 P and 0.87 P) are shown in Figure 4c.

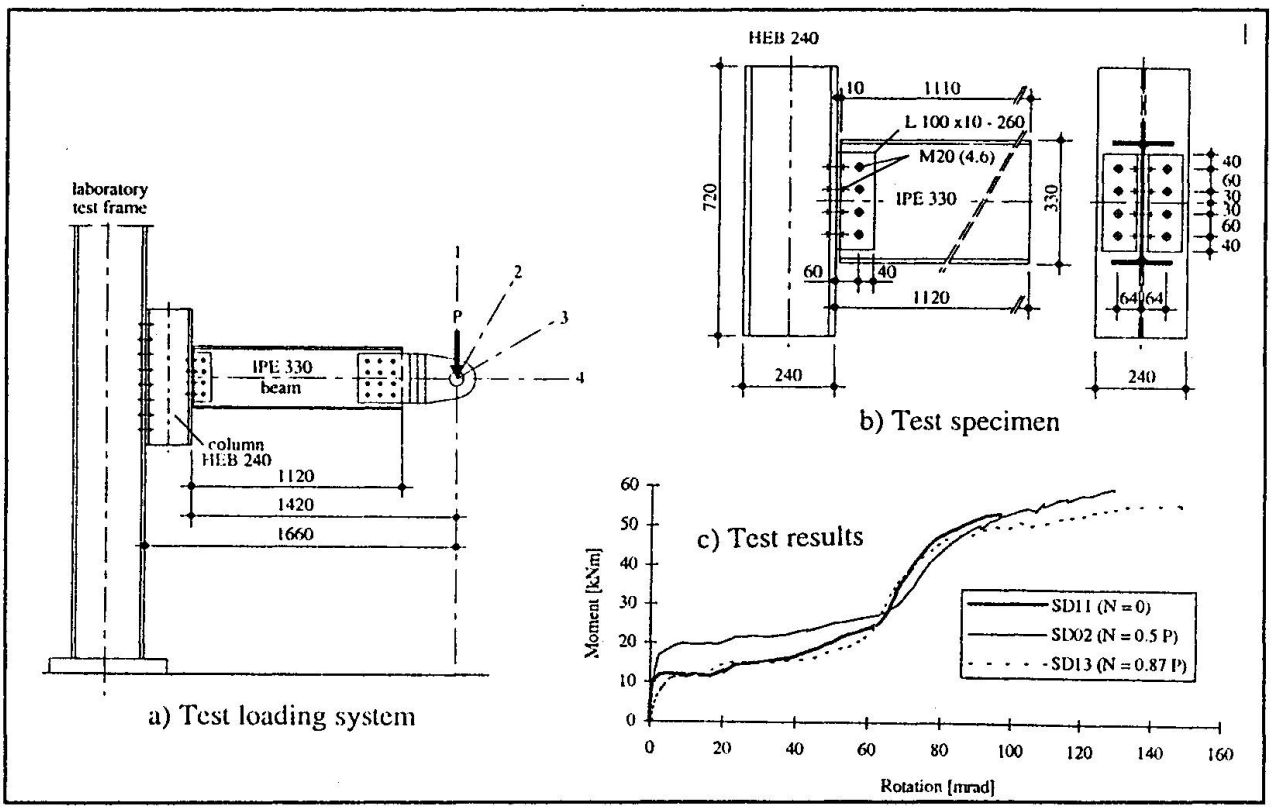

Fig. 4. Bare steel connection tests.

The moment-rotation behaviour of these three tests can be divided into three phases. The first was a initial elastic stage where no clear deformation occurred in the connection. The second

phase was characterised by a very long plateau with almost no change in moment resistance as rotation increased. The top of the beam clearly moved away from the column and the bottom of the beam clearly moved towards the column. Vertical slip was observed between the beam web and double cleats, without significant deformation of the cleats. The third phase started when the bottom of the beam touched the column flange. The stiffness increased and the web cleats started to deform significantly. The three tests were stopped by excessive deformation.

It is apparent from the moment-rotation curves that the joint in test SD11 (moment only applied), with the weakest components in the tension zone, had the lowest moment resistance. During test SD02 (low axial force applied) the neutral axis moved towards the critical components in the tension zone and the moment resistance was thus higher. Finally, during test SD13 (high axial force applied) the critical components moved from the tension to compression zone, so that moment resistance decreased again.

3.2 Composite joint tests

Two cruciform composite joint specimens were tested. Each specimen was composed of one column and two adjacent beams connected to the column using the same standard steel connection already described. The details of composite joint specimens are shown in Figure 5.

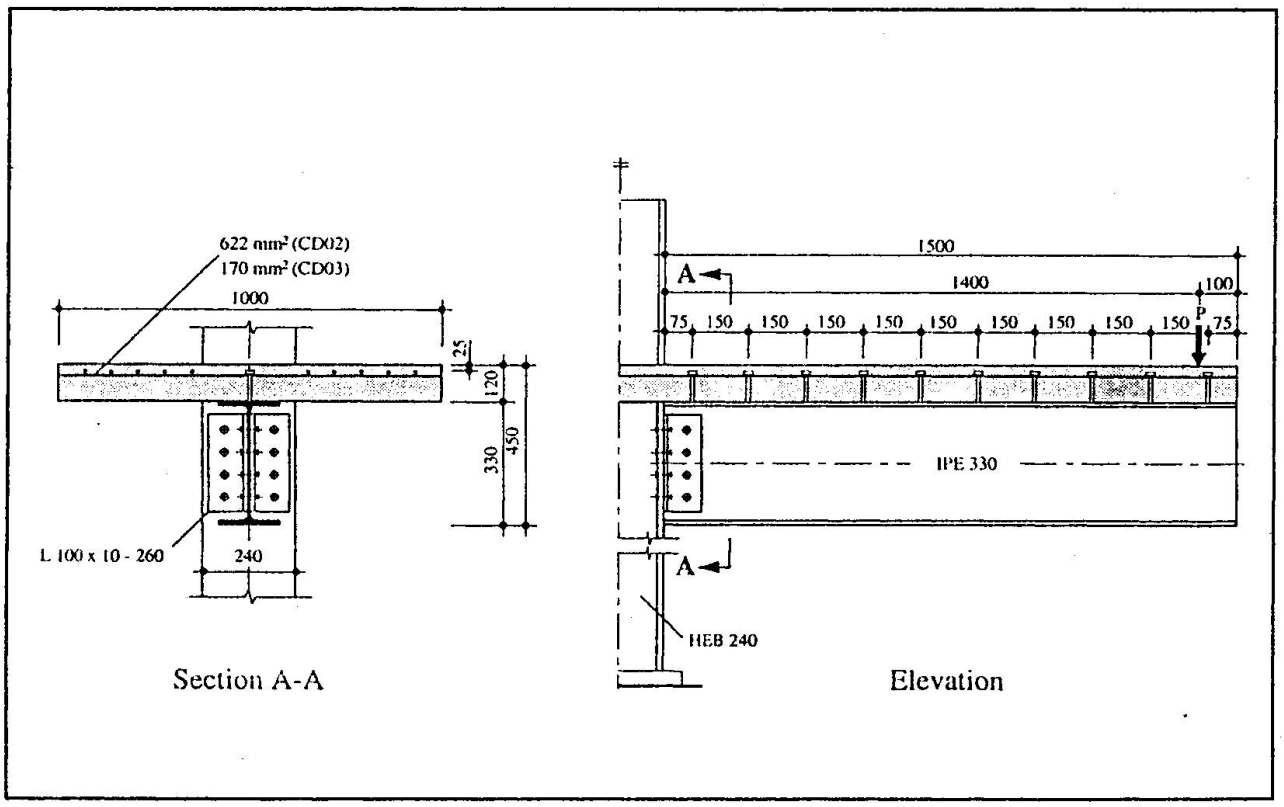

Fig. 5. Composite joint specimen.

The moment-rotation curves of the specimens tested are shown in Figure 6. Bare steel connection SD11 test results are given as a reference in the same figure.

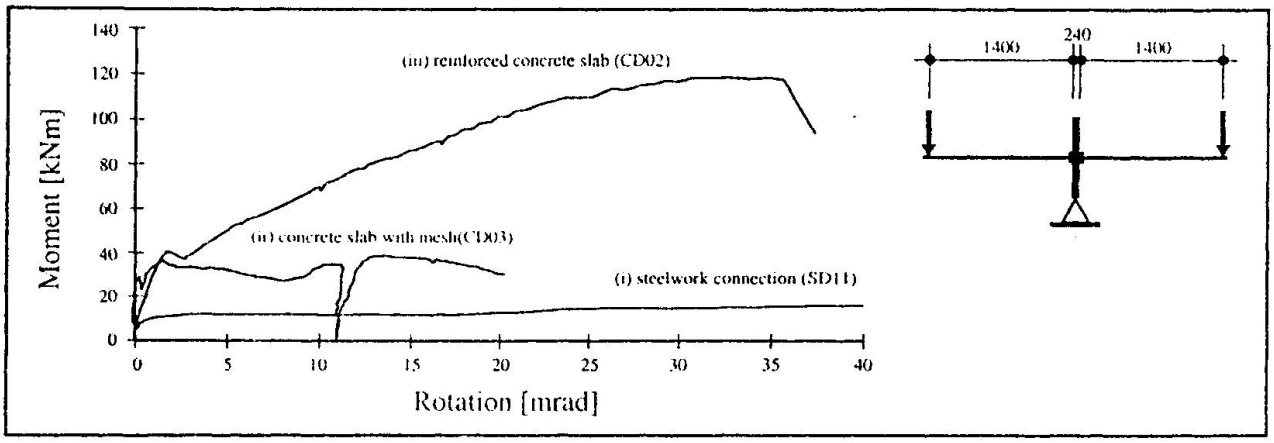

Fig. 6 Moment-rotation curves for composite joint tests.

Moment-rotation results of the first test (mesh and 4 x 12mm diameter rebars) exhibited a high moment resistance and good rotation capacity. With respect to much more deformation occurred in the steelwork connection, most of it being beam horizontal movement rather than rotation. Failure occurred also by the fracture of reinforcement at the cross-section through the column flange.

In the second test (mesh only), moment-rotation behaviour was characterised by a low moment resistance and small rotation capacity. Visible cracking in the slab was limited. No significant deformation occurred in the steelwork connection. Failure was due to mesh fracture at the cross-section through the column flange.

3.3 Analytical investigation

A numerical model of the non-linear composite joint behaviour including all flexibilities governing the characteristics of this type of joint has been developed [2]. By incorporating this numerical model into an existing composite beam analysis program [3], a new non-linear finite element (NLFE) program named COJOINT has been developed to simulate the semi-rigid behaviour of composite joints. This program has been verified with 14 tests of specimens having a wide range of member geometries, types of steelwork connections, degrees of horizontal shear interaction and reinforcement ratios [4]. The comparisons demonstrated a very good agreement between the tests and the numerical simulations. The relative importance of the parameters affecting composite joint behaviour has been identified by a parametric study with the use of the program COJOINT. This study enabled the development of the following simplified method.

4 Simplified method

4.1 Moment resistance

The method proposed for the prediction of the moment resistance of composite joints with double web cleat connections is similar to that for flush end plate connections, based on research undertaken in England [5, 6 and 7]. It is possible to use a plastic analysis (stress block method)

provided that the components of the joints have a ductile behaviour. The following simplifications are made when calculating negative moment resistance :

- tensile strength of concrete is neglected,
- moment resistance of the reinforced concrete slab is neglected,
- interaction between steel beam and concrete slab is complete,
- bolts in compression do not contribute to moment resistance, but they provide sufficient shear resistance,
- the resistance of the upper part of the connection in tension (bending and shear of the cleats, shear, bearing and tension of the bolts) is ignored,
- the centre of compression lies in the lower row of bolts,
- the resistance of the column web in compression is not critical.

Equilibrium is evaluated for the following internal forces (Fig. 7) :

- Tensile resistance of the reinforcement placed within the effective width of the concrete slab, F_s.
- Resistance of the zone in compression, F_c, represented by the shear or bearing resistance of the lower bolt in the web cleat connection.

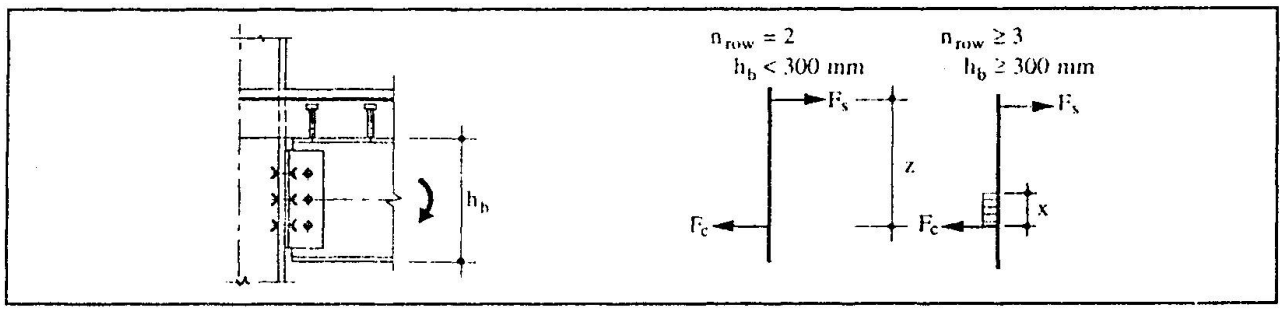

Fig. 7. Simplified model for composite joints with double web cleat connections.

Two cases can be defined according to the size of the elements.

First case : $h_b < 300$ mm $(n_{row} = 2)$

The moment resistance is then given by :

$$M_{Rd} = F \cdot z \tag{1}$$

F : minimum value of F_s or F_c
z : lever arm between compression and tension forces

Second case : $h_b \geq 300$ mm $(n_{row} \geq 3)$

If $F_c \geq F_s$, the moment resistance is given by Eq. (1), with $F = F_s$.
If $F_c < F_s$, a depth x of the web above the lower bolt is required to provide equilibrium :

$$x = \frac{F_s - F_c}{t_{wb} \, f_{yb}} \tag{2}$$

The moment resistance is then :

$$M_{Rd} = F_s \cdot z - (F_s - F_c)\frac{x}{2} \tag{3}$$

The transfer to the column flange of the force over the depth x is made using the bolts in the row above the lower row. The detailing of the third connection in Figure 4 illustrates a good solution for this force transfer. On the subject of the cross-sectional area of the total reinforcement (mesh + longitudinal bars), it should be chosen such that the neutral axis of the composite section lies within the web of the steel beam. In case of unbalanced moments, the area of the longitudinal reinforcement should be chosen such that failure of the section is ductile (Eurocode 4, Annex J [8]).

4.2 Rotational stiffness

The calculation of the rotational stiffness of composite joints is based on the following expression, derived from the formula proposed in the component method defined in Eurocode 4, Annex J [8]:

$$S_j = \frac{z^2}{\frac{1}{k_s} + \frac{1}{k_v} + \frac{1}{k_c}} \tag{4}$$

The stiffness of the reinforced concrete slab k_s is given by :

$$k_s = \frac{E_s \, A_s}{l_s} \tag{5}$$

E_s : modulus of elasticity of reinforcing steel
A_s : cross-sectional area of the total reinforcement (mesh + bars)
l_s : length of reinforcement under consideration (for example $l_s = h_c/2$) [7]
h_c : depth of the steel column

The stiffness of the shear connection k_v is given by :

$$k_v = \frac{\alpha F_v}{\delta_i} \tag{6}$$

α : reduction factor corresponding to the load at initial slip (for example $\delta_i = 0.1$ mm, see Figure 8)
F_v : longitudinal shear over the length of composite beam subjected to a hogging moment :

$$F_v = \min\left\{F_s \, , \, \sum P_{Rd}\right\} \tag{7}$$

$\sum P_{Rd}$: sum of the resistances of the shear connectors over the length of composite beam subjected to a hogging moment
δ_i : slip at the steel-concrete interface corresponding to the load $\alpha \, F_v$

Finally, the stiffness of the steel connection is given by :

$$k_c = \frac{E_a A_l n_{row}}{h_c / 2} \tag{8}$$

A_l : lateral bearing area of a bolt :

$$A_l = t_{wb} \cdot d \tag{9}$$

d : bolt diameter

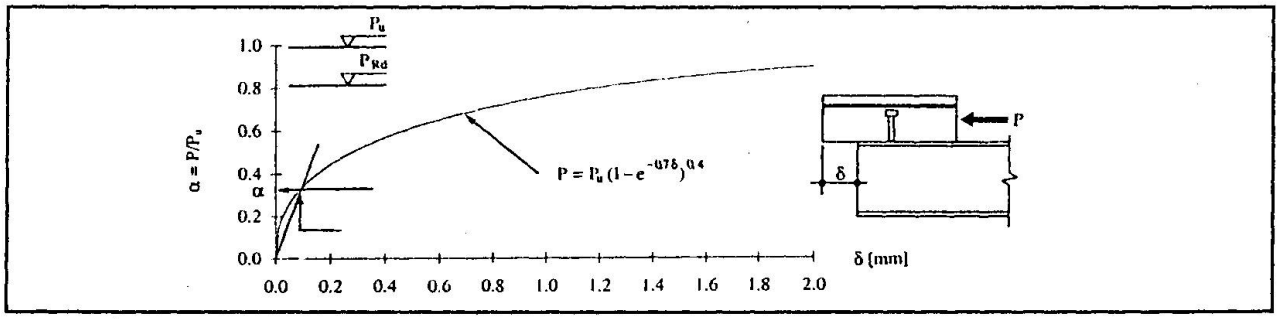

Fig. 8. Load-slip behaviour of a shear stud connector ([9]).

5. Comparisons

Figure 9 shows a typical comparison between test result of specimen CD02 and moment-rotation curves calculated with the NLFE COJOINT program and with the simplified method. The correlation between the experimental and the analytical behaviour is good in terms of initial rotational stiffness and moment resistance. However, the trilinear behaviour demonstrated in the test is difficult to reproduce by the "more exact" numerical model [2]. It can also be seen that the simplified method is conservative with respect to this model.

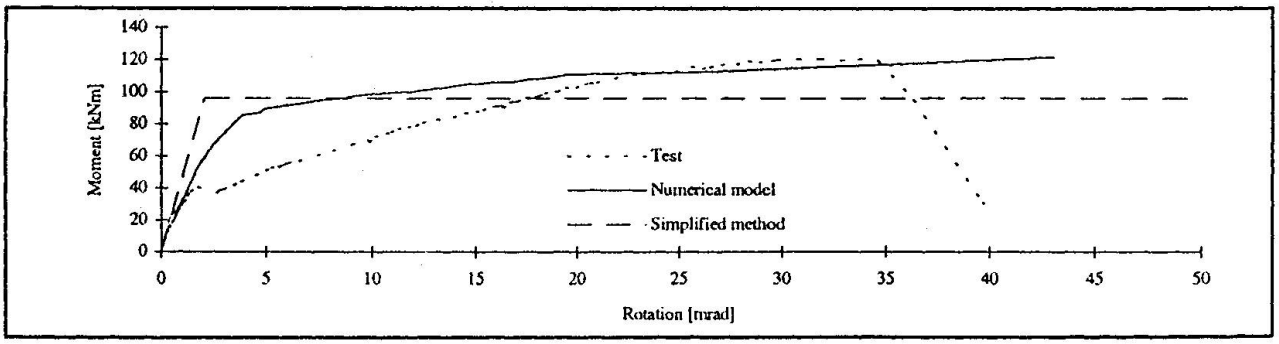

Fig. 9. Comparison between the test result, the numerical model and the simplified method.

Further comparisons have been conducted with several typical composite joints using different sizes of steel beam, web cleat, slab depth and reinforcement area (Fig. 10). The margin of safety is greater for small connections with only two rows of bolts than for large connections with three or more rows. This is due to the fact that the supplementary resistance existing in the actual connection is not taken into account in a small connection but is considered through the use of the x value in a larger one.

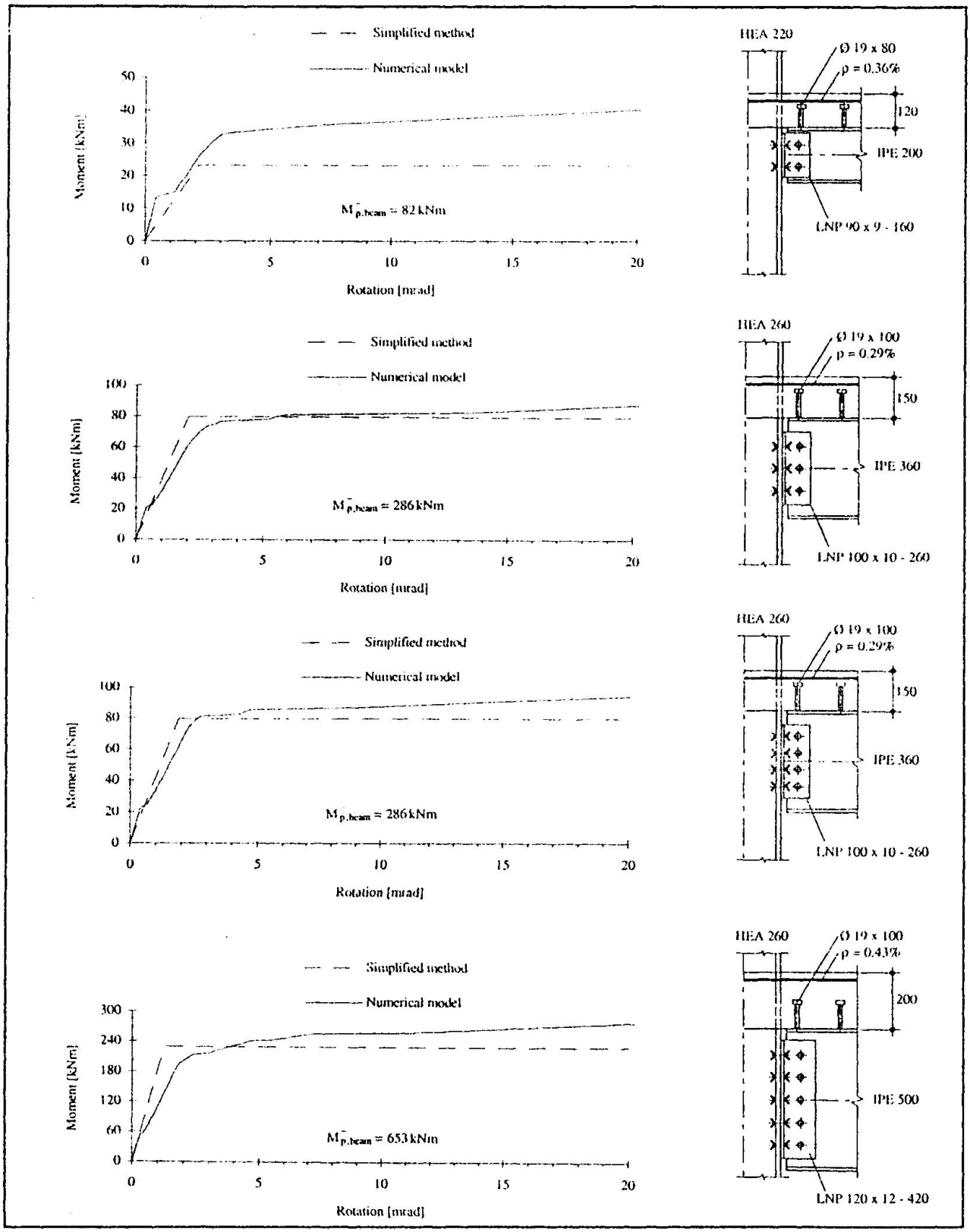

Fig.10. Comparison between the numerical model and the simplified method for four typical composite joints.

6. Conclusions

A method is proposed for the simple calculation of the moment resistance and rotational stiffness of standard double web cleat beam-to-column connections, taking account of the continuous reinforced concrete slab. This method is based on an existing method for end plate connections. Comparisons with test results and numerical simulations using a non linear finite element analysis show that the predicted behaviour is satisfactory. The contribution of the concrete slab enables the standard pinned steel beam-to-column connection to be considered as a semi-rigid composite joint. Bilinear characteristics determined by simple hand calculations can be easily used in the design of semi-continuous composite structures.

7. Acknowledgement

This study is part of a project sponsored by the Swiss National Science Foundation conducted in the framework of the European action COST C1 entitled "Semi-rigid Behaviour of Civil Engineering Structural Connections".

References

[1] SZS C9.1. La construction métallique, Assemblages par plaques frontales et boulons HR, Assemblages de poutrelles par doubles cornières, Appuis de poutres sans raidisseur. Centre Suisse de la Construction Métallique, Zurich, 1983.

[2] REN, P. Numerical modelling and experimental analysis of steel beam-to-column connections allowing for the influence of reinforced-concrete slabs. Ecole Polytechnique Fédérale de Lausanne, Thèse EPFL N° 1369, Lausanne, 1995.

[3] DANIELS, B. J., Comportement et capacite portante des dalles mixtes : Modélisation mathématique et étude expérimentale, Ecole Polytechnique Fédérale de Lausanne, Thèse EPFL N° 895, Lausanne, 1990.

[4] REN, P. and CRISINEL, M. Effect of reinforcement on the moment-rotation behaviour of standard steel beam-to-column joints. Proceedings of the Second State-of-the-Art Workshop COST C1, Ed. by F. Wald, Czech Technical University, Prague, 1994, pp 175-194.

[5] XIAO, Y., CHOO, B. S. & NETHERCOT, D. A. Composite connections in steel and concrete. I. Experimental behaviour of composite beam-column connections. J.Construct. Steel Research, Vol. 31, N°. 1, Oxford, UK, 1994, pp 3-30.

[6] ANDERSON, A. & NAJAFI, A. A. Performance of composite connections : Major axis end plate joints. J. Construct. Steel Research, Vol 31, N°. 1, Oxford, UK, 1994, pp 31-57.

[7] SCI 143. Moment connections in composite construction : Interim guidance for end-plate connections. The Steel Construction Institute, Technical Report, SCI Publication 143, Ascot (UK), 1995.

[8] EUROCODE 4 : Design of composite steel and concrete structures - Part 1 : General rules and rules for building. ENV 1994-1-1, European Committee for Standardization, Brussels, 1992.

[9] OLLGAARD, J. G., SLUTTER, R. G. and FISHER. J. W. Strength of stud connectors in lightweight and N°rmal-weight concrete. Engineering Journal, AISC, Vol. 8, N°. 2, Chicago, 1971, pp 55-64.

Leere Seite
Blank page
Page vide

THE EFFECT OF PLAIN BARS IN R/C BEAM-COLUMN JOINTS UNDER CYCLIC LOADING

Yılmaz YUVA
Assistant Professor
Department of Civil Engineering
Istanbul University, Avcılar
Istanbul, TURKEY.

received his Civil Engineering degree from Yıldız Technical University, Istanbul in 1985. He received his MS and PhD degrees from Boğaziçi University in 1989 and in 1996, respectively.

Gülay Altay AŞKAR
Professor and Head of Department
Department of Civil Engineering
Boğaziçi University, Bebek
Istanbul, TURKEY.

received her PhD in Civil Engineering in 1977 from Istanbul Technical University. Head of Civil Engineering Department since 1992 and Vice Dean of Engineering Faculty since 1995 in Boğaziçi University.

Summary

The research study presented herein is a part of the activities of Boğaziçi University involved in the (COST- C1) project. In scope of a collaborative research program between Boğaziçi University and CEC-JRC-ELSA, eight external beam-column joint subassemblages were tested in Ispra, Italy. The test results of three full-scale subassemblages fabricated using plain bars are presented herein. The results from the specimen tests were used to calibrate the hysteretic parameters of the code IDARC and a non-linear dynamic analysis of a low-rise reinforced concrete frame structure was performed under various effects using IDARC.

1. Introduction

The experimental part of the study is aimed to investigate the influence of the use of plain bars that have been used as main reinforcement in building construction in Turkey, to investigate the influence of joint transverse reinforcement on beam-column joint behavior and to investigate the behavior of adhesively bonded external steel plates under cyclic loading for the purpose of using this technique for structural members need to be strengthened in seismic regions.

In the analytical part, the results from the specimen tests were used to calibrate the hysteretic parameters of IDARC [1] which has been developed for inelastic damage analysis of reinforced concrete frame structures. Based on the results from the tests and other studies, non-linear dynamic analysis of an prototype reinforced concrete five-story frame structure, designed in accordance with the Turkish Codes, was performed using IDARC. Inelastic dynamic analysis for El Centro and Taft earthquakes were performed under various peak ground accelerations of 0.2g, 0.3g and 0.4g. The other variables are pinching parameter and P-Δ.

2. Experimental Program

Specimen configuration and testing methodology were similar for the entire full-scale component testing program involving experiments on bare and strengthened beam-column joints. Detailed experimental results are provided in [2][3].

All the specimens were so detailed that failure would occur in the beam. One of the specimens was detailed in accordance with the ACI "Recommendations" [4] and it will be named as "**ductile**". The specimen detail is shown in Figure 1. The second specimen was detailed as not conforming seismic detailing procedures on beam-column joints such as no transverse joint reinforcement, larger spacing of beam and column end region ties. The specimen will be named as "**non-ductile**" regardless of its behavior. The specimen detail is shown in Figure 2. The third one was detailed same as the "non-ductile" one and additionally, a strengthening scheme using adhesively bonded external steel plates was applied on the specimen to investigate behavior of this type of strengthening method under cyclic loading. The specimen will be named as "**strengthened**". The specimen detail is shown in Figure 3. The word "bare" is used as common for the "ductile" and "non-ductile" specimens.

2.1 Instrumentation

For all specimens, applied beam tip displacement and corresponding load, column axial load, eight transducer readings (four at beam end regions and four at column ends just above and below the joint region) were measured. In addition, 10 strain readings at "**non-ductile**" specimen, 12 strain readings at "**ductile**" specimen and 24 readings at "**strengthened**" specimen were measured.

Strains in the longitudinal, transverse and external reinforcements were measured at locations indicated in Figures 4, 5, and 6 for the "ductile", "non-ductile", and "strengthened" specimens, respectively. For the "strengthened" specimen, embedded strain-gauge locations are the same as the "non-ductile" specimen.

The testing system is shown in Figure 7. Displacement history applied at the beam end is shown in Figure 8. The locations of the LVDTs are shown in Figure 9.

2.2 Experimental Results

In this section, a brief summary of the observations recorded during the tests are presented.

2.2.1 Specimen BC1 "Ductile"

The specimen has the folowing characteristic details : Column reinforcement : 8ϕ14 continuous bars (not spliced), positive beam reinforcement : 3ϕ14 continuous bars, negative beam reinforcement : 3ϕ14 continuous bars, ties within the joint region : 6ϕ10, constant axial load on the column : 160 kN, measured average material strengths were f'_c= 19.3 MPa and f_y = 342 MPa, number of cycles applied : 27, number of recorded loading steps : 2700.

The first crack developed at the interface of the beam and joint panel. During the next cycles, the crack originating at beam end progressed further as reversing cyclic load was applied. The

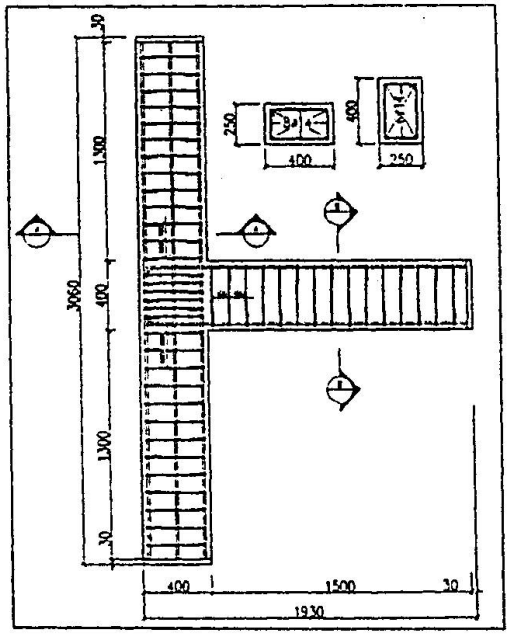

Figure 1. Details of Ductile Specimen

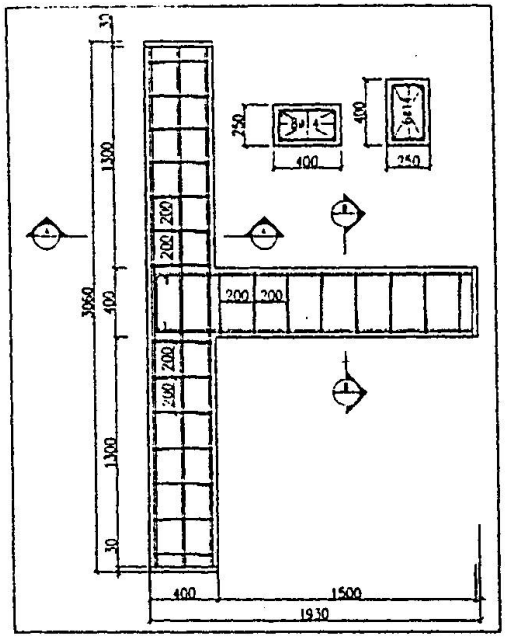

Figure 2. Details of Non-Ductile Specimen

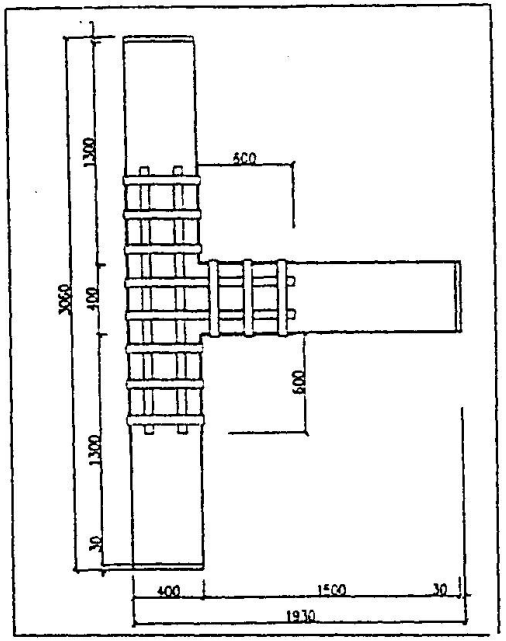

Figure 3. Details of Strengthened Specimen

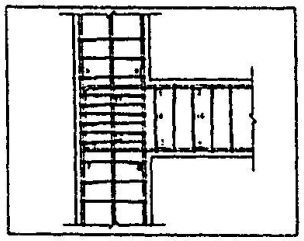

Figure 4. Strain-gages Ductile Specimen

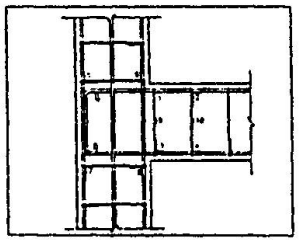

Figure 5. Strain-gages Non-Ductile Specimen

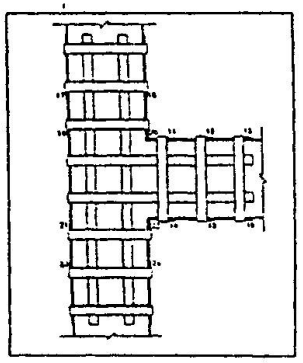

Figure 6. Strain-gages Strengthened Specimen

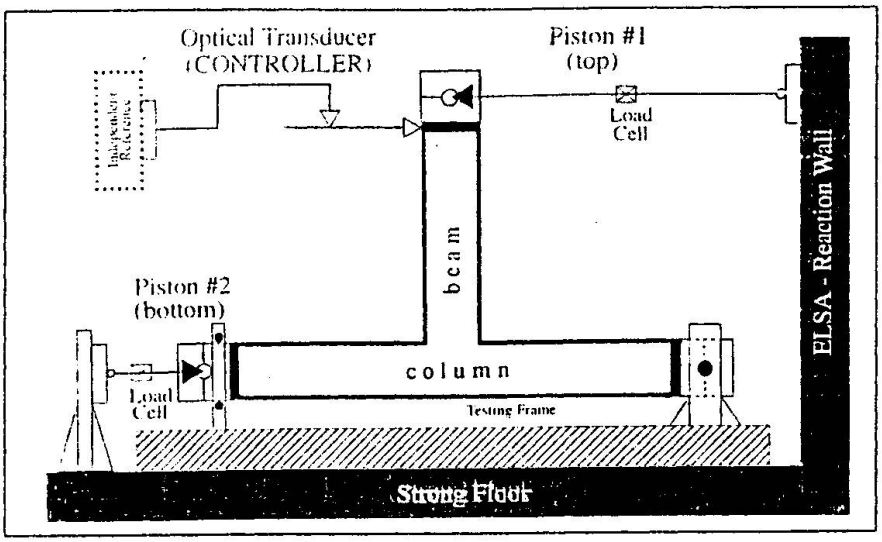

Figure 7. Schematic View of the Testing System

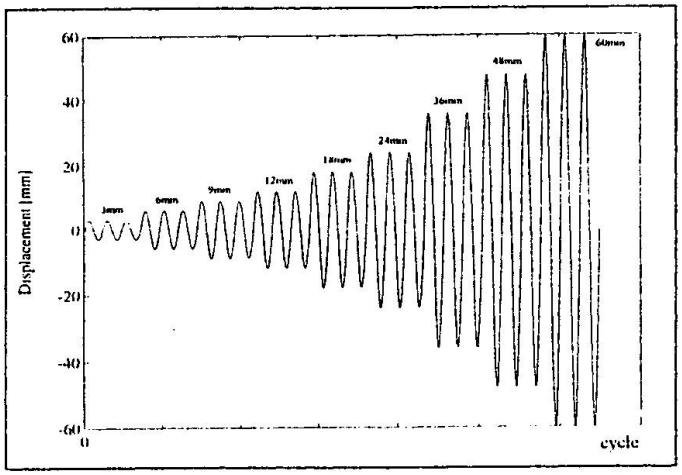

Figure 8. Loading History Applied at the Beam End

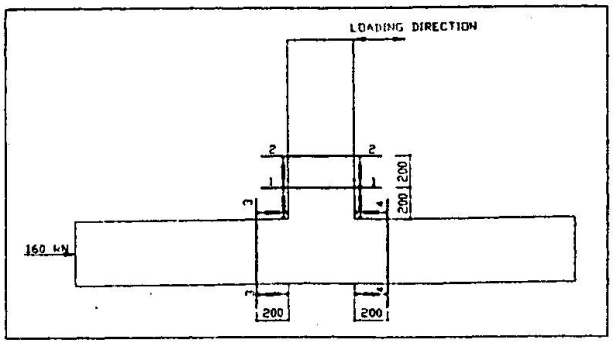

Figure 9. LVDT Locations

subsequent cycles caused further opening of this single crack. At 60 mm cycle, concrete cover spalling was initiated on the face opposite to the beam. No cracking was observed on the columns and the joint panel. The experiment was terminated when the crack was opened too much at 60 mm cycle and the LVDTs were contacted by spalling concrete cover.

2.2.2 Specimen BC'6 "Non-ductile"

The specimen has the folowing characteristic details : Column reinforcement : 8ϕ14 continuous bars (not spliced), positive beam reinforcement : 3ϕ14 continuous bars, negative beam reinforcement : 3ϕ14 continuous bars, no ties within the joint region, constant axial load on the column : 160 kN, measured average material strengths were f'_c= 18.3 MPa and f_y = 342 MPa, number of cycles applied : 25, number of recorded loading steps : 2500.

Observations for the "non-ductile" specimen are almost identical to the "ductile" specimen. However, concrete spalling at the outer face of the joint was observed on "non-ductile" specimen since the beam longitudinal bars tend to open in joint region under high load levels and no transverse joint reinforcement is available in the joint region.

2.2.3 Specimen BC'2 "Strengthened"

The specimen has the folowing characteristic details : Column reinforcement : 8ϕ14 continuous bars (not spliced), positive beam reinforcement : 3ϕ14 continuous bars, negative beam reinforcement : 3ϕ14 continuous bars, no ties within the joint region,external steel plates on the specimen, constant axial load on the column : 160 kN, measured average material strengths were f'_c= 22.1 MPa and f_y = 342 MPa, number of cycles applied : 22.5, number of recorded loading steps : 2250.

No crack was observed during the cycles of 3 mm and 6 mm. At the first cycle of 9 mm, a minor crack developed at the interface of the beam and joint panel, and also where the external plates are ended in the beam. The subsequent cycles caused further opening of the crack at beam plate end. For the safety of testing the experiment was terminated at one and a half cycle at 48 mm.

2.3 Load-Displacement Curves

The load-displacement curves are shown in Figure 10. The load values reached at extremes of 3 mm, 12 mm, 18 mm, 48 mm and 60 mm cycles are given averaging negative and positive displacement amplitudes as the following. At the first cycle of 3 mm for the "ductile", "non-ductile" and "strengthened" specimens, the measured load values are 12.88 kN, 14.02 kN and 21.68 kN, respectively. At the first cycle of 12 mm , the load values are 27.51 kN, 29.04 kN and 42.75 kN. For the "ductile" and "non-ductile" specimens, the load values are 29.12 kN and 29.04 kN, respectively, for the first cycle of 18 mm. For the "strengthened" specimen, a decrease in load level in tension side of the beam at the first cycle of 18 mm was observed. The measured load value at the third cycle of 12 mm is 38.95 kN while it is 38.36 kN at the first cycle of 18 mm. Instead of an increase in load level due to increase in displacement amplitude, approximately 1.5 percent decrease was measured. This can be attributed to partial seperation of the external plates from the concrete surface. Because of this decrease in tension side of the beam at the first +18 mm displacement amplitude the load values for the subsequent cycles are not given for the "strengthened" specimen. At the first 48 mm cycle, the load values are 30.34 kN and 30.42 kN. At the first cycle of 60 mm, the load values are 30.52 kN and 30.75 kN.

As seen from the load displacement curves, all three specimens are almost stabilized the load level after yielding, only slight strength degradation is observed for all specimens tested. The strength degradation is around 4 percent for each repeated cycles of same displacement amplitude. In other words, strength degradation between first and third cycle of same amplitude is around 8 percent.

2.4 Energy Dissipation

Taking the "ductile" specimen hysteretic energy dissipation as the reference (i.e. 100%), energy dissipation values for the other two specimens are given as the following. Hysteretic energy dissipated corresponds to the cumulative dissipated energy for the three repeated cycles of same displacement amplitude. For all three cycles of 3 mm, energy dissipation is 122% and 189% for the "non-ductile" and "strengthened" specimens, respectively. For all 3 mm and 6 mm cycles, the values are 86% and 151%. For the nine cycles up to 12 mm cycle, the values are 68% and 123% for the "non-ductile" and "strengthened" specimens, respectively. For the twelve cycles up to 18 mm cycle, the values are 69% and 111% for the "non-ductile" and "strengthened" specimens, respectively. It can be concluded from the dissipated energy values obtained from the tests in this study that energy dissipation in strengthening by using externally bonded steel plate technique decreases with increase in ductility. In other words, in high ductility demand, the strengthening technique does not provide significant contribution to energy dissipation capacity.

Hysteretic energy curve for the three experiments is shown in Figure 11. As shown from the figure that the most energy dissipation is occurred for the strengthened specimen. With regard to bare specimens, ductile specimen dissipated more energy than the non-ductile specimen.

3. Analytical Study

For the calibration of the load-displacement behavior of the bare specimens a parametric study was performed playing with IDARC Ver. 3.1 hysteretic parameters. The parametric study results are provided in [2]. The analytical load-displacement curve capturing the experimental load-displacement curve is shown in Figure 10.d.

3.1 Prototype R/C Frame Structure

In this study, to examine the influence of beam-column joints on the overall behavior of reinforced concrete frame structures during earthquakes a typical bent of a five-story frame structure was chosen as a case study. Only one way framing scheme of the model structure was considered.

3.2 Nonlinear Analysis of Prototype Structure

An analysis was made to determine the likely mode of failure (beam or column hinging, or joint failure) at each connection region in the model structure. The purpose of the analysis was to identify the weakest element of each connection region. The code IDARC Ver. 3.1 was used for the inelastic analysis of the structure. Two sets of IDARC parameters were defined for

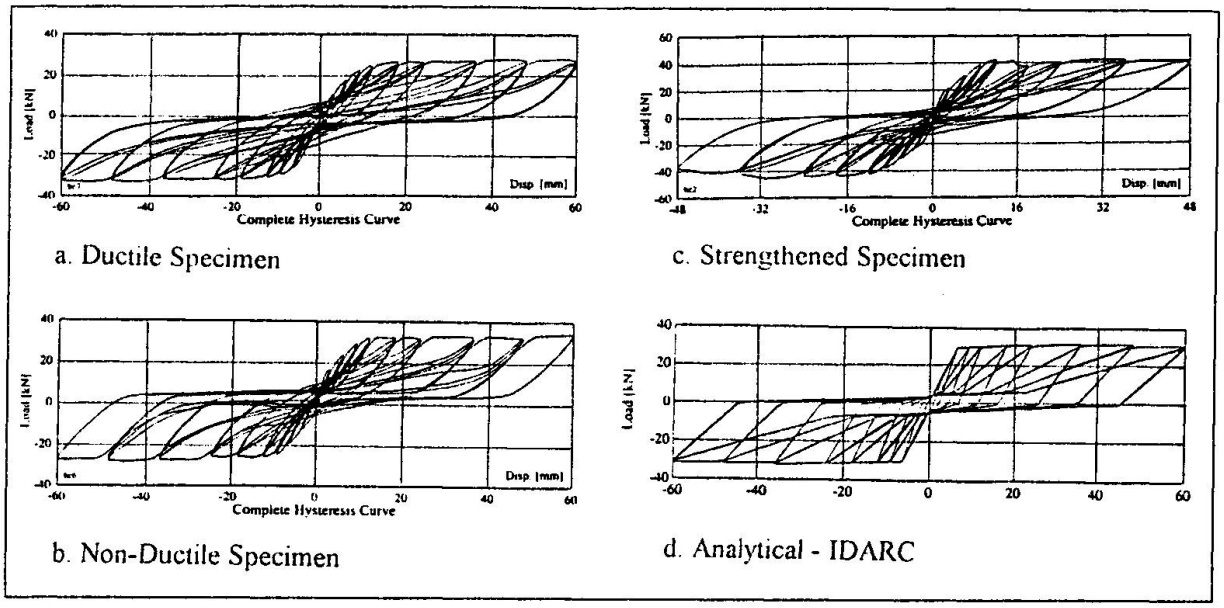

Figure 10. Load-Displacement Curves

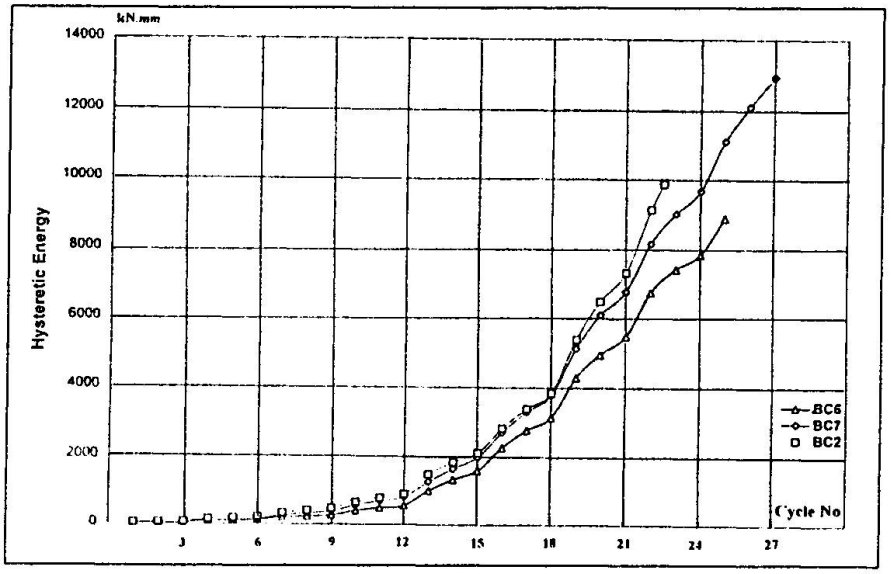

Figure 11. Hysteretic Energy Curves

the whole structure. One set of hysteretic parameters was provided for each end of beam and column members. The variables to be examined are the influences of P-Δ effect, bond characteristics of reinforcing steel and type of earthquake.

From a monotonic push-over analysis, which is an inverted triangular static loading on the structure until the drift level is achieved, based on a 2% top story drift limit of the total height of the structure a base shear capacity of 14% of the total weight W is computed.

IDARC is used to estimate the critical peak ground acceleration to scale the El Centro S00E and Taft S69E components to induce collapse on the example frame structure. The criteria used to determine the critical peak ground motion are related to the following variables: **i.)** base shear demand and capacity, **ii.)** the maximum interstory drifts, **iii.)** the damage index of the critical story columns and of the overall structure.

For this analytical evaluation, repetitive analyses were done using the El Centro 1940 S00E and Taft 1952 S69E earthquakes with the PGAs of 0.2g, 0.3g and 0.4g.

From nonlinear dynamic analyses, the story shears, story displacements and maximum interstory drifts for various PGAs of 0.2g, 0.3g and 0.4g were obtained. Including P-Δ effect, the maximum computed base shears for the El Centro earthquake are 301.2 kN (10.11% W), 388.3 kN (13.03% W), and 434.3 kN (14.57% W). For the Taft earthquake the values are 336.7 kN (11.3% W), 401.8 kN (13.48% W), and 432.6 kN (14.52% W) for the PGA values of 0.2g, 0.3g and 0.4g, respectively. Therefore, according to the model, the base shear capacity has been achieved in the 0.4g for both the El Centro and Taft Earthquakes with and without P-Δ effect.

For the El Centro S00E motion, the interstory drifts are exceeded for the 0.3g and 0.4g PGAs on the fifth floor. The interstory drift maxima for the first four stories remain within tolerable limits. The fifth floor drift values are 2.68% and 3.51% of the story height for the 0.3g and 0.4g PGAs without P-Δ effect. Including P-Δ effect, the values become 2.89% and 4.49%, respectively. The base shear demands are about 73% of capacity, 94% of capacity for the 0.2g and 0.3g PGAs, respectively. For the 0.4g PGA base shear demand reaches capacity.

Interstory drifts obtained during Taft S69E component are within reasonable limits. Only the fifth story drift value for the 0.4g PGA exceeds 2%. (2.24% and 2.17% of the story height with and without P-Δ effect, respectively). For this case, it can be said that P-Δ has no great influence on the structural performance with regard to maximum displacements, maximum interstory drifts and base shear capacity. However, the base shear force demands approach capacity very rapidly. For the 0.2g motion, the base shear demand is about 80% of capacity. For the 0.3g motion, the base shear demand is about 96% of capacity. For the 0.4g motion, the base shear demand reaches capacity. Therefore, collapse is very probable for the 0.30g PGA and inevitable for the 0.40g PGA.

The damage model in IDARC assesses the level of damage induced in the structure both at the component and story levels. This model assigns a damage index value between 0.0 and 1.0, with 0.0 indicating no damage and 1.0 representing total collapse.

Most of the damage occurs to the columns of the fifth floor. The maxima damage indices are 0.28 and 0.69 for the 0.2g and 0.3g PGAs, respectively. The damage index reaches severe damage state for the 0.3g motion. Also the overall structural damage indices for the 0.2g and 0.3g motions are 0.128 and 0.249, respectively, which indicate minor damage. Finally at 0.4g, the damage index for the fifth floor columns is between 0.98 and 1.02. Therefore, collapse of the top story columns is definite with 0.4g. Also the overall structural damage index for this motion is 0.361, which indicates moderate damage. Therefore from the response results and corresponding critical members and overall structural damage indices from IDARC, it is determined that the El Centro S00E component with a PGA of 0.4g would induce collapse of the fifth story columns. The resulting collapse mechanism is a column-sidesway mechanism.

The third criteria for determination of the critical PGA for collapse of the example structure is the damage index of the members and of overall structure. For the Taft earthquake, most of the damage occurs to the fifth story columns. Thus the resulting failure mechanism is that of column-sidesway collapse mechanism. The damage index maxima for the fifth story columns are 0.21, 0.35 and 0.54 for the 0.2g, 0.3g and 0.4g PGAs, respectively. The overall structural damage index values for the 0.2g, 0.3g and 0.4g PGAs are 0.105, 0.177 and 0.269, respectively. It can be concluded that the damage indices for the member and for the overall structure remain within minor through moderate-repairable damage state.

So far, all the results from IDARC are obtained using the pinching hysteretic parameter corresponding to plain bar obtained in this experimental study. Additional results are obtained with 0.3g PGA for both the Taft and the El Centro motions. The new pinching parameters are considered to simulate bond characteristics of the deformed reinforcing steel. In that case, most of the damage occurs to the columns of the fifth floor for the El Centro S00E motion. The damage indices are between 0.53 and 0.58 for the top story columns. In comparison to the damage indices obtained in the original case (i.e. using plain bar hysteretic pinching parameter) , the damage indices are decreased. Furthermore, the overall structural damage index is 0.237 which is less than 0.249. For the Taft earthquake, the damage indices are greater than 1.0 for all fifth story columns while the maxima is 0.35 with the original hysteretic parameters. Therefore, collapse of the fifth story columns is definite for 0.3g motion.

4. Conclusions and Recommendations

1. As in the current Code, the new draft Turkish Earthquake Code expected to be in use in 1996 does not contain any provisions and recommendations pertaining to the use of deformed bars. As clearly seen from the load-displacement curves that severe pinching occurs in use of plain bars. The draft Code therefore should restrict the use of plain bars as main reinforcement in the 1st and 2nd degree earthquake zones in Turkey.
2. It can be concluded from the "ductile" and "non-ductile" subassemblage tests results that for the cases with high flexural strength ratio and low joint shear stress, joint transverse reinforcement could be reduced without jeopardizing the performance of the frame.
3. It was observed from the results of the tests that high pinching occurred due to the weak bond behavior of plain bars although the specimens were designed in accordance with ACI "Recommendations". For the hysteretic behavior modeling purposes, the pinching factor in IDARC may be taken as around 0.2 even if the joint is in elastic range.

4. From the analytical study performed in this study, it has been realized that damage level at member level and for the entire system is very sensitive to hysteretic parameters chosen. Structure behavior is not influenced much by the hysteretic parameters. Mechanisms that will cause damage/failure (or collapse) at member level should be clearly identified prior to make a decision for the parameters.
5. Much more experimental study should be performed to determine more efficient plate dimensions and configuration, and also to understand all aspects of externally bonded steel plate technique under earthquake type loading. One conclusion can be drawn from the strengthened specimen test in this study that the plate length extending from column face to beam should be reduced (extend between one half of beam height - beam height).
6. The failure of strengthened beam-column subassemblage was occurred in the beam section where the external plates are ended, not at the column face as in the cases of bare specimen tests. Repair and strengthening work near joint region is much more difficult and joint failure influences the behavior of a member of a frame significantly. Methods to relocate plastic hinges away from joints is getting popularity to avoid the difficulties mentioned above. The strengthening technique applied in this study may be used an alternative method to move plastic hinges to an appropriate location.

Acknowledgement

The authors are grateful to the Boğaziçi University Research Fund and the Boğaziçi University Foundation for their support on the project. The first author is grateful to TÜBİTAK (The Scientific and Technical Research Council of Turkey) for the scholarship to carry out the experimental and analytical studies at ELSA Laboratory, Ispra , Italy and Cornell University, Ithaca, New York, the USA, respectively.

References

1. Kunnath, S.K., Reinhorn, A.M., IDARC-2D - Version 3.1 - Inelastic Damage Analysis of RC Building Structures, September, 1994.
2. Yuva, Y. " Experimental and Analytical Study on the Seismic Behavior of Reinforced Concrete Frame Structures ", PhD Dissertation, Department of Civil Engineering, Boğaziçi University, 1996, Istanbul, Turkey.
3. Köylüoğlu, A.M., Yuva, Y., Aşkar, G.A., Verzeletti, G. and A. Pinto, Seismic Strengthening of R/C Joints Using Adhesively Bonded Steel Plates - Experimental Results, Report EUR 16276 EN, European Commission, Joint Research Center, Safety Technology Institute, European Laboratory for Structural Assessment, 1995.
4. ACI-ASCE Committee 352, (1976,1985,1991), Recommendations for Design of Beam-Column Joints in Monolithic Reinforced Concrete Structures, American Concrete Institute, Detroit, MI.

Semi-rigid behaviour of beam-to-column minor-axis joints

Luís COSTA NEVES
Civil Engineer, Msc
University of Coimbra
Portugal

Fernando GOMES
Civil Engineer, Msc
University of Coimbra
Portugal

Luís Costa Neves, born 1968, got his civil engineering degree from the University of Coimbra in 1992 and his Master from the same University in 1996, where he is assistant since 1992. His research interests are mainly in the field of semi-rigid behaviour of steel structures.

Fernando Gomes, born 1955, got his civil engineering degree from the University of Coimbra (where he is assistant) in 1978 and his Master from the Technical Univ. of Lisbon. His research interests are mainly in the field of semi-rigid behaviour of steel structures, and he is national representative of european project COST C1.

Summary

The behaviour of beam-to-column minor-axis joints is characterised by a non-linear moment-rotation curve with possible high stiffness and moment capacity. Although models to evaluate the strength of the column web based on curved yield lines are available, there are no means of predicting analytically its stiffness. A numerical study highlighting the major parameters determining the stiffness is described. Finally, simple formulae to predict initial, secant and membrane stiffness, based on the numerical study and on a physical model are given.

1. Introduction

The rotational behaviour of a minor-axis joint may be characterised, as any other joint, by the behaviour of its basic components: bolts, cleats, end plate, column web loaded out of its plan. This is the design philosophy of EUROCODE 3 [2], as explained on its annex J, and known as "component method". For the type of joint covered by this paper, EUROCODE 3 gives application rules for the characterisation of all components but one, that plays a fundamental role: the column web loaded out of its plan, which typical moment-rotation $(M-\phi)$ curve is shown in Fig. 1. Also shown are the main geometrical characteristics of such joint.

Rotational behaviour of the column web in a minor axis joint may be characterised by the determination of several key parameters: plastic moment (M_{pl}), rotation capacity (ϕ_{pl}) and stiffness (S) corresponding to a given moment level. Studies recently published by Gomes [3], [6], and by Gomes, Jaspart and Maquoi [5] give quite accurate methods to predict the plastic moment, based on curved yield lines. It has also been shown, namely in [4], that these joints generally have a good rotation capacity. As stiffness is concerned, a distinction has to be made (Fig. 1) between elastic or initial stiffness (S_i), secant stiffness (S_j) - namely to the plastic moment - and membrane stiffness (S_m) - that characterises the post-plastic behaviour. There aren't, on the author's knowledge, proposals for the prediction of these stiffnesses. Nevertheless, there are some general studies, mainly related to RHS, that could identify relevant parameters. CZECHOWSKI *et al* [1], propose some formulae to predict the initial stiffness of a RHS joint, problem that may be, in some circumstances similar to a minor-axis joint.

The evaluation of those joint stiffnesses has been the objective of a research program started three years ago at the University of Coimbra and which conclusions have been recently published [10]. Due to the large number of parameters involved, it is difficult to obtain analytical direct solutions; a parametric finite element study has then been conducted, and its results were used to propose simple formulae and to calibrate simple physical models.

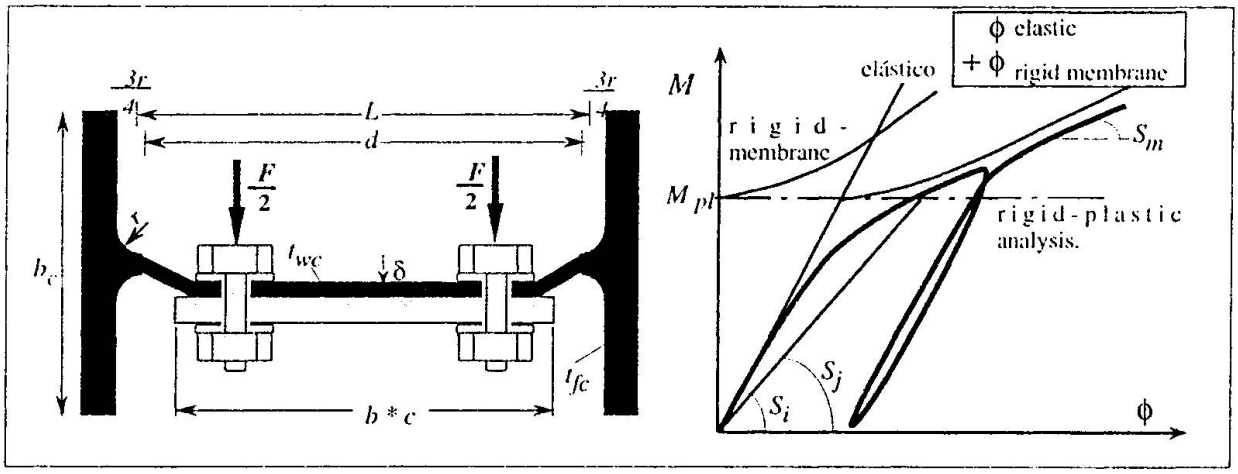

Fig. 1 - Column web in a minor-axis joint; geometrical characteristics and typical behaviour

2. Characterisation of web deformation - Parametric study

Relevant parameters considered in this study are:

- Type of web's failure mechanism: local - Fig. 2a (involving one of the forces composing the bending moment transmitted from the beam) and global - Fig. 2b (involving those two forces). Local mechanism occurs for large values of h (Fig. 2c) and global mechanism for small values of h.. Non-dimensionally, this may be controlled by the parameter $\gamma = h/L$. Boundaries between these two types of mechanisms have been defined by Gomes [3].

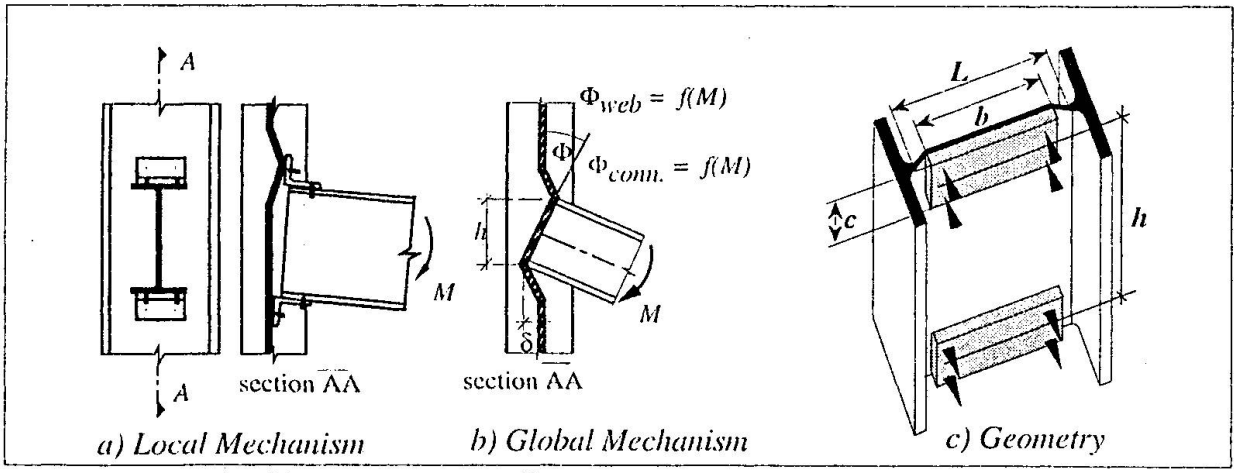

Fig. 2 - Types of yielding mechanism and relevant geometrical parameters

- Dimensions $b \times c$ of the loaded area (Fig. 1 and 2c), to which correspond, respectively, the non-dimensional parameters $\beta = b/L$ and $\alpha = c/L$.

- Slenderness of the column web, defined by the parameter $\mu = L/t_{wc}$ (Fig. 1), and that plays a fundamental role in the post-plastic behaviour of this joint component. For commercial hot rolled sections of IPE and HE series, μ varies approximately between 10 and 50.

- Restraint offered by the column flanges to the web's rotation; two situations have been considered:

i) tridimensional joint, Fig. 3a, where major-axis beams prevent rotation of the column flanges. In this situation the column web may be modelled as a plate clamped at the junction with the flanges.

ii) minor-axis joint alone, Fig. 3b, where the column flanges are free to rotate. Restriction to the web's rotation may be expressed by a parameter ψ, that depends on the section geometrical characteristics - Fig. 1;

$$\psi = \frac{\left(\frac{L}{t_{wc}}\right)}{\left(\frac{b_c}{L}\right)\cdot\left(\frac{t_{fc}}{t_{wc}}\right)^3} \qquad (1)$$

where $\psi = 0$ corresponds to a clamped web at the junctions with the flanges. Variation of factor ψ for sections of the European series IPE and HE has been presented in [10]. In this parametric study both values of $\psi = 0$ (corresponding to a tridimensional joint) and $\psi = 22$ (that covers reasonably well and on the safe side European commercial series) have been considered.

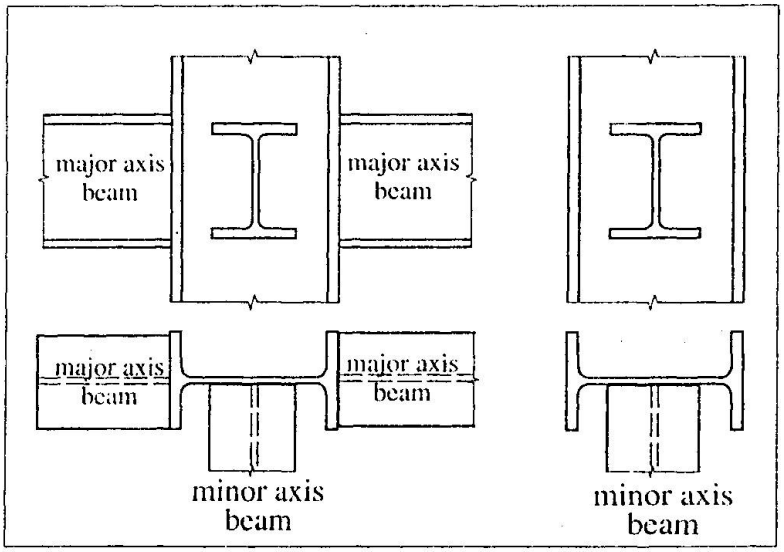

Fig. 3 - (a)Restrained and (b)unrestrained column flanges.

The study has been conducted using the finite element package LUSAS, modelling the column web with eight-noded thick shell elements (LUSAS elements QTS8). Four noded (QTS4) and triangular thick shell elements (TTS6 and TTS3) have also been used respectively in low stress areas and to assure transition between different mesh densities.

Ranges of variation for the different parameters were: $0{,}08 \le \beta \le 0{,}75$, $0{,}05 \le \alpha \le 0{,}2$, $10 \le \mu \le 50$, $0{,}5 \le \gamma \le \infty$. Material has been considered to be elastic-perfectly plastic, according to the von Mises yield criterion. Three types of analysis have been performed: elastic, elasto-plastic, and second-order elasto-plastic. Only this last type of analysis may follow all the moment-rotation (or force displacement) curve shown in Fig. 1. Differences between 1st and 2nd order analysis result from membrane effects, that considerably increase with parameter μ; thinner webs develop more important second order effects.

Further details on this numerical model may be found in [9] and [10]. Its validation has been made comparing: (a) qualitatively general options and results from other works, (b) values obtained for the plastic load F_{pl}, from elasto-plastic first order analysis in the full range of parameters studied, with the theoretical values proposed in [5]. From this comparison a maximum error of ± 5% has been observed. Finally, (c), full non-linear second order curves have been compared with some experimental tests from [4], showing a good agreement between experimental and numerical curves [10].

3. Initial stiffness, S_i

3.1 Fully restrained flanges

The initial (or elastic) stiffness is the initial slope of $M-\phi$ (or $F-\delta$) curve - Fig. 1. From the observation of finite element results in the elastic range, it could be concluded that the web may be modelled as a plate supported at the junction with the flanges and free in the other borders. This model, represented in Fig. 4, has a length equal to L (Fig. 1) and a width l_{eff} that depends on the dimensions of the loaded area:

$$l_{eff} = c + (L-b)\tan\theta \qquad (2) \qquad \frac{l_{eff}}{L} = \alpha + (1-\beta)\tan\theta \qquad (3)$$

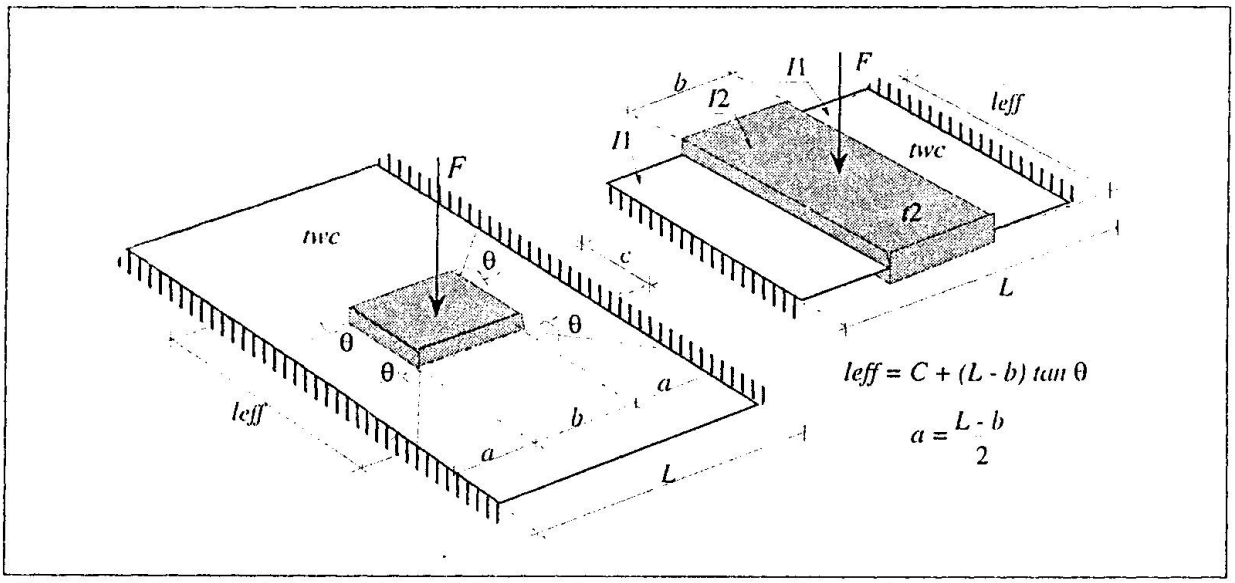

Fig. 4 - Column web loaded by a rigid area $b \times c$, and equivalent strip of width l_{eff}.

Initial stiffness of this strip, computing both flexural and shear deformations, may be easily expressed by:

$$S_i = \frac{2E\, l_{eff}\, t_{wc}^3}{a^3 + 2(1+\upsilon)a\, t_{wc}^2} \quad ; \quad a = \frac{1}{2}(L-b) \qquad (4)$$

Substituting the value of a and l_{eff} given by eq. (2), taking Poisson's coefficient $\upsilon = 0{,}3$, it is obtained, after introduction of two coefficients k_1 and k_2:

$$S_i = \frac{E\, t_{wc}^3}{L^2} \cdot 16 \frac{\alpha + (1-\beta)\tan\theta}{(1-\beta)^3 + \dfrac{10{,}4(k_1 - k_2\beta)}{\mu^2}} \tag{5}$$

L and t_{wc} are given in Fig. 1, $\alpha = c/L$, $\beta = b/L$, $\mu = L/t_{wc}$, and E is the young modulus.

The term $10{,}4(k_1 - k_2\beta)$ represents the contribution of shear effects to the initial stiffness, and it is shown in [10] that plays an important role for thick webs. Introduction of coefficients k_1 and k_2 is justified from the different influence of shear effects for small values of μ on the model and on the numerical simulations, and thus to correct that effect. Their most convenient values have been shown to be $k_1 = 1{,}5$ and $k_2 = 1{,}63$. Angle θ, from which depends the strip width, results from the condition that initial stiffness of strip model must be equal to the initial stiffness obtained from the finite element analysis, $S_{i,\mathrm{adim}}^{Sim}$ (non-dimensional).

$$\theta = \tan^{-1}\left[\frac{S_{i,\mathrm{adim}}^{Sim}}{16}\left((1-\beta)^2 + \frac{10{,}4}{\mu^2}\frac{(k_1 + k_2\beta)}{(1-\beta)}\right) - \frac{\alpha}{1-\beta}\right] \tag{6}$$

We could verify [10] that angle θ may be approximated, without significant error, by a linear function of β alone:

$$\theta = 35 - 10\beta \tag{7}$$

This proposal for the initial translational stiffness of the column web in a minor-axis joint (for local or global mechanism) is compared in Fig. 5a to 5c with the results from the numerical simulations, for some of the $\mu = L/t_{wc}$ values considered.

In each case initial stiffness is non - dimensionalized with respect to Et_{wc}^3/L^2, and different curves correspond to different values of α. A good agreement could be found between results obtained from application of eqs. (5) and (7) and those obtained from numerical simulations, with a maximum error in the range of parameters studied of 3% and 9%, respectively on the unsafe and on the safe side.

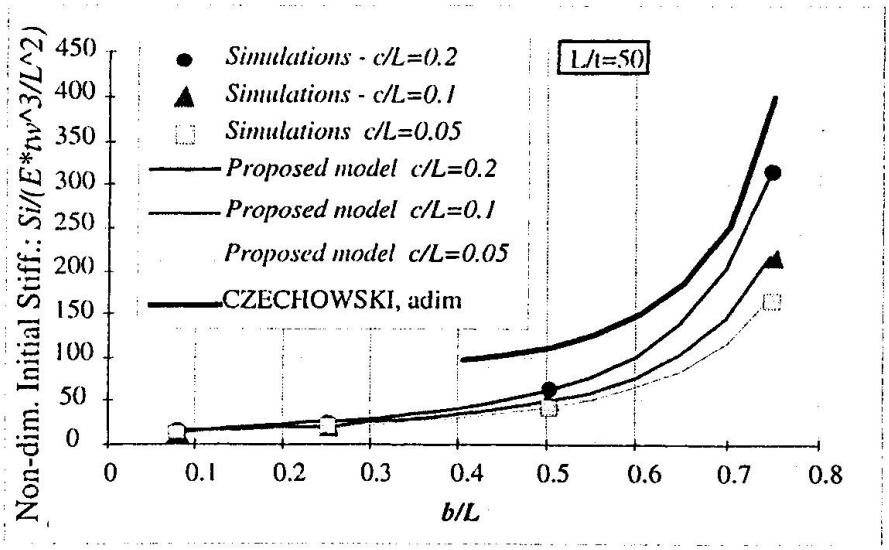

Fig. 5a

Also shown is the proposal of Chechowski [1] for the elastic stiffness of a RHS joint, in a situation similar to the column web in a minor-axis joint [10].

Chechowski's model largely overestimates elastic stiffness, specially for small values of slenderness, μ.

Rotational stiffness, S_i^{ϕ}, may be calculated from translational stiffness, by:

$$S_i^{\phi} = \frac{M}{\phi} = \frac{h^2}{\frac{1}{S_{i1}} + \frac{1}{S_{i2}}} \quad (8)$$

where h is the distance between centres of superior and inferior loaded areas (Fig. 2c), with translational stiffnesses S_{i1} and S_{i2}, calculated from eqs. (5) and (7).

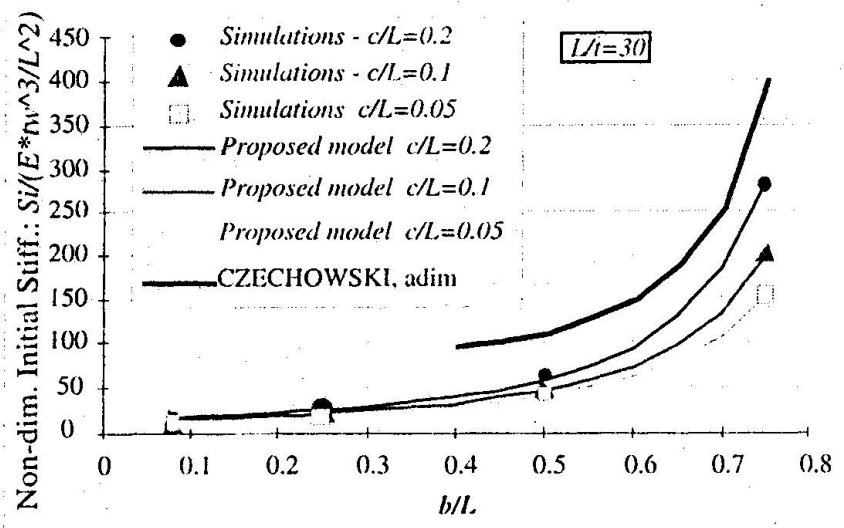

Fig. 5b

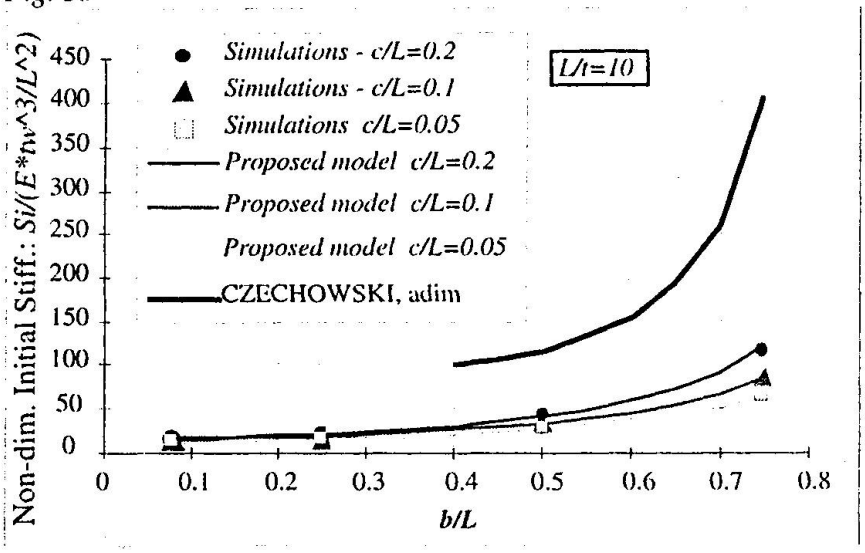

Fig. 5 c

Fig. 5 - Variation of initial translational stiffness with geometrical parameters. Comparison between proposal model, numerical simulations and Czechowski's model

3.2 Column flanges with rotational freedom

Fig. 6 compares non-dimensional rotational stiffness plotted against coefficient β and for different values of α, for fully restrained flanges (Fig. 3a) and for flanges with rotational freedom (Fig. 3b). Initial stiffness decreases with flange rotation. This decrease is more significant for bigger loaded areas, and may be characterised by the coefficient k_{rot}, ratio between initial stiffness for free and restrained flanges [10]:

$$k_{rot} = \frac{S_{i,rot}}{S_i} = \begin{cases} 0,52 - 0,40\beta & - \text{ for HE sections bigger than HEA 400, HEB 500, HEM 600, and IPE sections} \\ 1 & - \text{ for HE sections smaller or equal to HEA400, HEB500, HEM600} \end{cases} \quad (9)$$

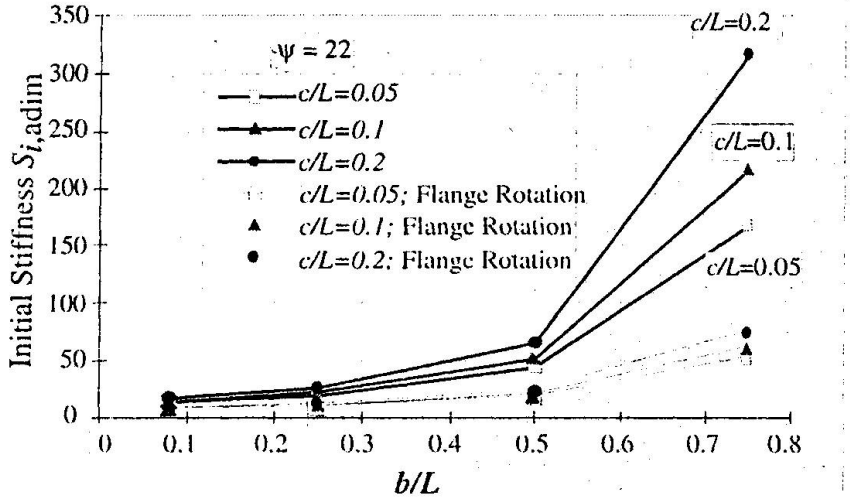

Fig. 6 - Effect of flanges rotation on initial stiffness

4. Secant stiffness, S_j

Annex J of EUROCODE 3 [2] gives a simple way to determine secant stiffness, S_j, to use if $M_j \geq 2/3 M_{j,Rd}$ (i.e. if the moment acting on the joint is greater or equal to 2/3 of its resistant moment), dividing the initial stiffness, S_i, from a coefficient η, given on that annex for the types of joints actually covered. For the column web in a minor axis joint, we propose:

$$S_j = \begin{cases} \dfrac{S_i}{\eta} & \text{– Restrained flanges or column section smaller or equal to HEA 400, HEB 500 or HEM 600} \\ \dfrac{S_i}{\eta_{Rot}} & \text{– Unrestrained flanges and section greater than HE 400, HEB 500, HEM 600 or IPE sections} \end{cases} \quad (10)$$

where η is a function of β (table 1) and $\eta_{Rot} = 2/3\,\eta$. Fig. 7 shows an example of application of eq. (10) to the curves resulting from numerical simulations for $\beta = 0{,}5$ and $\alpha = 0{,}2$.

β	η
≤ 0,25	2
0,5	3
0,75	5

Table 1 - Values of η function of β

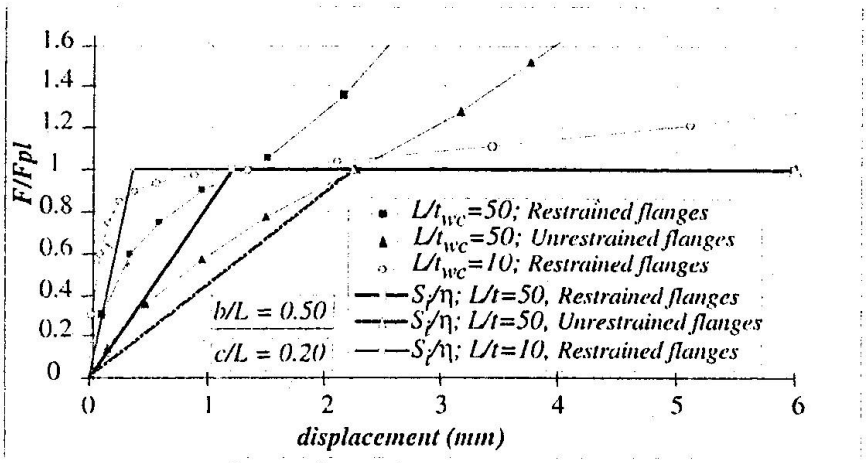

Fig. 7- Curves $F/F_{pl} - \delta$ for $\beta = 0{,}5$ and $\alpha = 0{,}2$

5. Post-plastic behaviour

The column web in a minor-axis joint is a plate loaded by the forces equivalent to the applied bending moment. According to Massonnet [7], there are theoretical results available to predict second order behaviour of certain strips and circular plates, characterised by a parabolic curve followed by a linear function. From some experimental studies [7] it may be concluded that force-displacement curves for bigger span / thickness ratios (where second order effects are more important) are steeper than those corresponding to smaller values of that ratio. However, if those curves are non-dimensionalized with respect to the plastic force and to the plate's thickness (i.e. transformed in curves $F/F_{pl} - \delta/t$) curves are approximately parallel in their straight parts. We could verify from our numerical simulations that those results apply to a column web in a minor-axis joint, and that the displacement corresponding to the transition between the parabolic curve and the straight line is approximately the thickness of the column web. These facts led us to propose [10] a model to characterise the post-yielding behaviour of the column web, which is important to evaluate its overstrenght, that could lead to brittle failure of non-ductile components (bolts or welds). This model is showed in Fig. 8, and the two straight lines are fully characterised by two parameters: f_2 or non-dimensional membrane stiffness $\left(S_{m,a\,\mathrm{dim}}\right)$ and f_1 or intersection with F/F_{pl} axis of the straight part or $F/F_{pl} - \delta/t$ curve;

$$\frac{F}{F_{pl}} = \begin{cases} 0{,}9 + (f_1 + f_2 - 0{,}9)\left(\dfrac{\delta}{t}\right) & \text{if } \dfrac{\delta}{t} \le 1 \text{ and } \dfrac{F}{F_{pl}} \ge 1 \\ f_1 + f_2\left(\dfrac{\delta}{t}\right) & \text{if } \dfrac{\delta}{t} \ge 1 \text{ and } \dfrac{F}{F_{pl}} \ge 1 \end{cases} \tag{11}$$

From our parametric study we could propose for f_1 and f_2:

$$f_1 = -0{,}24\beta - 0{,}012\mu + 0{,}72 \qquad (12) \qquad f_2 = 0{,}55 + 1{,}07\alpha + 0{,}85 \qquad (13)$$

which have showed to lead to a safe estimate for the post-plastic limit of the column web.

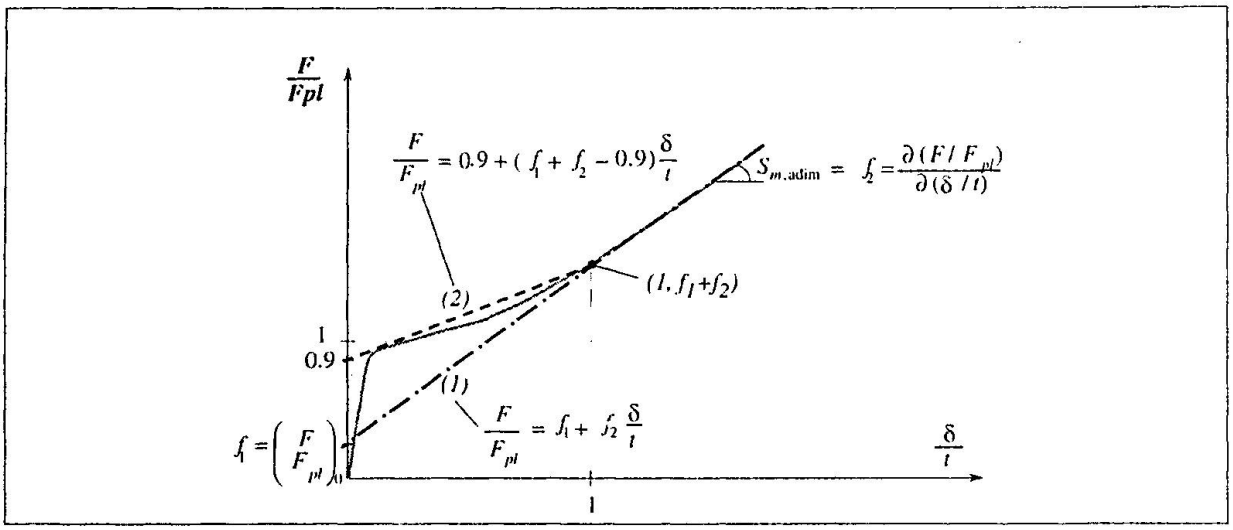

Fig. 8 - Bi-linear approximation of column web post-limit behaviour

6. Conclusions

A parametric study conducted using the finite-element method led to the identification of the major parameters influencing the behaviour of the column web in a minor-axis joint.

The elastic (or initial stiffness) may be evaluated by simple formulae that are based on a physical model - strip plate, and corrected by the numerical simulations results. The presented proposal leads to a good estimation of the observed numerical results and constitutes a considerable improvement to previous models.

Secant stiffness may be computed by dividing initial stiffness from a η coefficient that has been obtained from the numerical simulations.

Finally, post-yielding behaviour may be approximated by a bi-linear model based on two parameters - membrane stiffness, and intersection with F/F_{pl} axis of the straight line that characterises post-yielding behaviour for large deflections. A proposal for those parameters based on numerical simulations has been made, and leads to a safe estimation of column web overstrenght.

7. References

[1] CZECHOWSKI, A., KORDJAK, J., BRÓDKA, J., Flexibility Formulae and Modelling of Joint Behaviour in Girders made of Rectangular Hollow Sections. *Proceedings of a state-of-the-art workshop on Connections and the Behaviour, Strength and Design of Steel Structures held at the ENS, Cachan, May 1987*, Elsevier Applied Science, London, 1987, pp 175-182.

[2] EUROCODE N° 3 - Design of Steel Structures. Part 1.1: General Rules and Rules for Buildings - European Prestandard ENV 1993-1-1, Commission of the European Communities, Brussels, 1992.

[3] GOMES, F.C.T., Etat Limite Ultime de la Résistance de L'âme d'une Colonne dans un Assemblage Semi-Rigide d'axe Faible, Rapport Interne n° 203, MSM - Université de Liège, Août 1990.

[4] GOMES, F.C.T., JASPART, J.-P., Experimental research of minor-axis joints. Comparison with theoretical predictions, COST C1 WG2 Meeting, Coimbra, Nov. 1994. Doc. COST C1/WD2/94-13.

[5] GOMES, F.C.T., JASPART, J.P., MAQUOI, R., Behaviour of Minor Axis Joints and 3-D Joints, *Proceedings of the second state-of-the-art workshop on Semi-Rigid Behaviour of Civil Engineering Structural Connections, Prague, Out. 1994.*

[6] GOMES, F.C.T., Moment capacity of beam-to-column minor-axis joints, *Proceedings of the IABSE International Colloquium on Semi-Rigid Structural Connections, Turkey, Sept. 1996.*

[7] MASSONET, SAVE, Calcul Plastique des Constructions - vol II Structures Dépendant de Plusieurs Paramètres, ASBL, Bruxelles, 1972.

[8] NEVES, L.F.C., GOMES, F.C.T., Parametric study on the behaviour of minor-axis joints, COST C1 WG2 Meeting, Coimbra, Nov. 1994. Doc. COST C1/WD2/94-?.

[9] NEVES, L.F.C., GOMES, F.C.T., Numerical simulation of a column web in a minor-axis joint, COST C1 WG6 Meeting, Trento-Italy, July 1995. Doc. COST C1/WG6/95-?.

[10] NEVES, L.F.C., Nós semi-rígidos em estruturas metálicas. Avaliação da rigidez em configurações de eixo fraco (in portuguese), Thesis submitted in partial fulfillment of the requirements for the degree of Master of Structures, Coimbra, 1996